Measurement based Tapped Delay Line Model for Train-to-Train Communications

Erislandy Mozo, Paul Unterhuber, *Member, IEEE*, Arrate Alonso Gómez,
Stephan Sand, *Senior Member, IEEE*, Mikel Mendicute, *Senior Member, IEEE*

***Abstract*—Train-to-train (T2T) communication is proposed as an auxiliary safety-guaranteed measure for railway communications. Vehicular communication standards have been supporting railway use cases and T2T communications. It is essential to consider the propagation characteristics of railway environments with dedicated T2T channel models for simulation and testing of vehicular communication standards. In this paper, we propose six tapped delay line (TDL) channel models for T2T communications in Hilly Terrain and Railway Station. The measurement based proposed channel models consider different T2T distances and relative speeds of up to 50 km/h with trains moving in an approaching maneuver. Also, a study about the Doppler-delay behavior in the considered scenarios is presented using the scattering function. The proposed TDL channel models as well as the measured propagation characteristics are used in a 802.11bd simulation framework. Both simulation results, which are based on the TDL channel models or on the measurements, are compared to each other. The results show a very good match between the TDL channel models and the measurement data and indicate a good accuracy of the theoretical derivations and the simulation method.**

***Index Terms*—channel model, tapped delay line, railway, Doppler spread, 802.11bd, train-to-train communication, Doppler-delay spectrum.**

I. Introduction

Train-to-train (T2T) communications have won attention in the last decade, where several research projects have been carried out to modernize railway communications. It allows a reliable radio link that is capable of transferring data directly between trains. Then, this T2T link can handle safety critical data traffic with low end-to-end latency compared to a centralized system. In this way, trains can exchange information about their composition, position, relative speed and train length among others. T2T communications are foreseen as the enabling technology of new railway applications, which will allow to improve train safety, availability, and operation. Critical applications such as collision avoidance, decentralized communications-based train control (CBTC), and train composition coupling are under investigation [1].

E. Mozo, A. Alonso-Gómez, and M. Mendicute are with the Signal Theory and Communications Group, Electronics and Computer Science Department, Mondragon Unibersitatea, Arrasate-Mondragon, Spain.

P. Unterhuber and S. Sand are with Institute of Communications and Navigation, German Aerospace Center (DLR), Oberpfaffenhofen, 82234 Wessling, Germany.

Corresponding author: E. Mozo (e-mail: erislandy.mozo@gmail.com).

Commercial technologies such as C-V2X, TETRA, 802.11, and WiMAX have capabilities to support T2T links. For instance, the analysis of ITS-G5 based on 802.11p was presented in a T2T link under high speed railway (HSR) conditions [2]. In addition, new communication protocols are being standardized which enable use cases in railway scenarios since a part of the 5.9 GHz band has been assigned for railway purpose. The successor of 802.11p, 802.11bd will add new advanced processing techniques to its physical layer [3]. Another one is NR-V2X, which is expected to be standardized in the current release (17) by the 3rd Generation Partnership Project (3GPP).

The performance evaluation of the previous mentioned wireless technologies requires accurate channel models and measurement campaigns carried out in railway scenarios. In [4], the authors provide a rich literature analysis of existing railway channel models based on measurement only for train-to-infrastructure (T2I) communications. Some tapped delay line (TDL) channel models are identified and used to evaluate the performance of the Emulradio4Rail platform [4]. Also, the WINNER II model is a TDL model used by 3GPP for railway applications with frequencies up to 6 GHz [5].

Several channel models, measurement campaigns and propagation studies have been carried out for T2I communications [6], [7]. In comparison, only a few studies have been reported for T2T communications and a research gap is observed. The first studies in relation to T2T communications based on measurements were carried out in [8], [9], [10]. These articles cover different radio phenomena in the 400 MHz band which include path loss, Doppler shift, fading, and delay spread. In [11], a geometric channel model is presented for a viaduct T2T environment in the 900 MHz band. The wireless channel is characterized with the path loss, the k-factor and the covariance of the envelope. Please note that the channel models shown in [8] and [11] were not tested with a communication system to validate its performance, and they are valid for frequency bands below 1 GHz.

In addition, some measurement campaigns have been carried out to characterize the propagation phenomenon in T2T scenarios and the results have been reported in [2], [12], [13]. In [14], a wideband channel sounding was performed in the 5.9 GHz band. Then, time-variant statistical parameters of the T2T channel were derived for different use cases and driving maneuvers. Also in [15], the authors present an exhaustive study of time-varying stochastic channel parameters for different scenarios, and how the propagation characteristics vary with the T2T distance and the selected scenario.

From the literature, it is observed that no T2T railway

scenario is represented by a model that can be used for simulation and evaluation of the radio link performance in the 5.9 GHz band. The contributions of this paper can be summarized as follows:

- We derive six tapped delay line channel models available for T2T communications based on measurements, which cover different T2T distances and two railway scenarios (Hilly Terrain and Railway Station).
- We analyze the stochastic channel parameters and the Doppler-delay behavior of T2T channel at short, medium, and large distances in the considered scenarios.
- We show and evaluate the 802.11bd performance in railway scenarios using the proposed channel models for different modulation and coding schemes (MCS).

A. Organization of the paper

The paper is organized as follows: In Section II, the measurement campaign carried out by DLR is briefly described, as well as the procedure followed to extract the channel parameters from the measurement data. Next in Section III, the TDL models are introduced for T2T scenarios and results are shown. Finally, the TDL models are validated in Section IV, and the conclusions are presented in Section V.

B. Notation

In this paper, a scalar is denoted by a, the i^{th} element of a column vector is denoted by $a(i)$, and the $(i,j)^{th}$ element of a matrix by $a(i,j)$. In addition, $a(\cdot)$ is used for continuous parameters, while $a[\cdot]$ is used for discrete parameters. The magnitude and the estimated value of a are denoted by $|a|$ and $\hat{a}$, respectively. The estimate of the expectation of a random variable X is denoted by $\hat{\mathbb{E}}[X]$. The smallest integer that is greater or equal than $a \in \mathbb{R}$ is denoted by $\lceil a \rceil$, being $\mathbb{R}$ the set of real numbers.

II. Railway Channel Measurements and Analysis

Modelling the wireless channel is one of the most difficult tasks of radio system design, and is usually done in a statistical way, based on measurements made specifically for an intended communication system and spectrum allocation. The channel models are generally based on a mathematical representation of the impulse response of a multipath channel $h(t,\tau)$, where t and τ represent time and delay, respectively. $h(t,\tau)$ contains all information required to simulate or analyze any type of radio transmission through the channel.

A baseband representation for $h(t,\tau)$ was given by [16] as:

$$h(t,\tau) = \sum_{i=0}^{M-1} a_i(t,\tau) e^{j\theta_i(t,\tau)} \delta(\tau - \tau_i(t)), \qquad (1)$$

being $\theta_i(t,\tau) = 2\pi\eta_i(t,\tau)\tau_i + \phi_i(t,\tau)$ the total phase term. The terms $a_i(t,\tau)$, $\phi_i(t,\tau)$, and $\tau_i(t)$ represent the real amplitude, phase, and delay of the i^{th} multipath component encountered in the channel at time t, respectively. The M phase components $\phi_i(t,\tau)$ are mutually independent random variables uniformly distributed over [-π; π], where M is the number of multipath components in the channel including the first arriving or line-of-sight (LoS) component. Moreover, δ(t) is the Dirac-delta function. Each multipath component experiences a Doppler frequency $\eta_i(t,\tau)$ due to dual mobility of the transmitter and receiver [17, page 42], which has associated an angle of arrival $\alpha_i(t,\tau)$.

In addition, $\alpha_i(t,\tau)$ includes the arrival direction and the movement direction, and whose statistical distribution determines the power spectral density or Doppler spectrum of $\eta_i(t,\tau)$. For instance, when $\alpha_i(t,\tau)$ exhibits a uniform distribution [4], the Doppler spectrum is represented by the "Jakes" spectrum. Then, the Doppler frequency of LoS component is expressed as:

$$\eta_{\text{los}}(t,\tau) = \frac{\Delta v f_{\text{c}}}{c} \cos\left(\alpha_{\text{los}}(t,\tau)\right), \qquad (2)$$

where Δv represents the relative speed, f_{c} represents the carrier frequency of the transmitted signal, and c is the speed of light. Also, the term $\alpha_{\text{los}}(t,\tau)$ represents angle of arrival of LoS component. Some topics, definitions and assumptions are examined in the next four subsections, which will be used throughout this manuscript.

A. Measuring impulse response

Using a channel sounder, it is possible to obtain a band-limited discrete representation for $h(t,\tau)$, denoted by $h[n,m]$, being n and m the time and delay indices. The last result is normally taken sampling the impulse response $h(t,\tau)$ at equidistant time intervals Δt and at samples spaced $\Delta\tau$ in the delay domain. The delay resolution $\Delta\tau = 1/W$ takes into account the sampling theorem, where W represents the measurement bandwidth used in the channel sounder. Then, the discrete representation of the band-limited baseband wireless channel in a geographic area S is given by

$$h[n,m] = \sum_{i=0}^{N_{\text{b}}-1} a_i[n,m] e^{j\theta_i[n,m]} h_{\text{BL}}(m\Delta\tau - \tau_i[n]), \qquad (3)$$

where N_{b} represents the total number of bins of the channel sounder, $\theta_i[n,m]$ represents the total discrete phase term, and $a_i[n,m]$ represents the discrete amplitude term. Also, $h_{\text{BL}}(\tau)$ is the convolution of the band-limiting filters used at the transmitter and receiver side in the channel sounder.

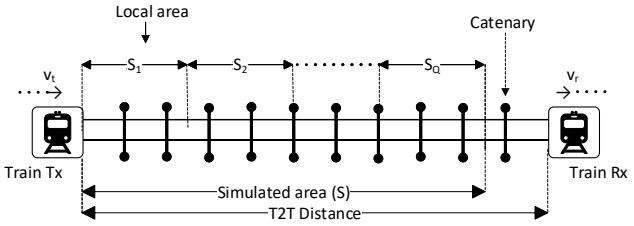

Fig. 1. Simulation model for a approaching maneuver based on local areas.

In vehicular communications, the received signal fades due to the mobility and the multipath propagation conditions. The fading can be described by a non-stationary process, in which the channel statistics including $h[n,m]$ can change within

a rather short period of time [18]. As a result, the implementation of (3) can not be performed assuming wide-sense stationary uncorrelated scattering (WSSUS) for longer periods of time. To manage this drawback, the fading process can be considered locally stationarity for a local area or stationary region S_q with finite extent in time, where $q = 1, \cdots, Q$ represents the local area index [19], and Q the total number of local areas in S. For instance, Fig. 1 shows how a geographic area S is divided into Q equally spaced areas S_q. Please note, S is the disjoint union of all S_q, such that $S = S_1 \cup S_2 \cdots \cup S_Q$.

The last approach is possible because the channel parameters change with a finite rate which usually represents a stationary distance d_s in the range of 20λ to 40λ, where $\lambda = c/f_\mathrm{c}$ represents the wavelength of the received signal [20]. The stationary time $t_\mathrm{s} = d_\mathrm{s}/\Delta v$ used in this article is chosen based on [15], where a stationarity analysis was carried out using the same data set and scenarios as in this article.

The measured impulse response in q^{th} local area is given by

$$h[n', m; q] = h[(q-1)N_\mathrm{s} + n', m], \tag{4}$$

where $n' = 0, \cdots, N_\mathrm{s} - 1$ is the time index in a local area, and $N_\mathrm{s} = \lceil t_\mathrm{s}/\Delta t \rceil$ is the number of measured impulse responses in a local area. Then, $h[n', m; q]$ represents a subset of $h[n, m]$ located in the q^{th} local area and limited by the time interval $[(q-1)N_\mathrm{s}; qN_\mathrm{s} - 1]$. This approach has been used in [19] to describe the non-stationary behavior of the channel using the local scattering function $P[n, m; q]$. In our case, we use $P[n, m; q]$ to estimate the scattering function $\hat{P}[n, m]$ as the average of all $P[n, m; q]$ calculated in S.

B. Scattering function

In this subsection, we are particularly interested in characterizing the dispersion of the received signal through the wireless channel in the Doppler-delay domain. The estimation of the Doppler-delay spectrum, called scattering function in [21], is essential for this target. The scattering function $P[m, d]$ is a two-dimensional function of the propagation delay index m and the Doppler index d.

The procedure for calculating $P[m, d; q]$ from the measurement data consists of two steps as described in [14], where the WSSUS assumption is assumed for each local area [15] based on t_s which is calculated for each analyzed propagation scenarios. First, the local Doppler-variant impulse response is calculated using the discrete Fourier transform by

$$s[m, d; q] = \frac{1}{N_\mathrm{s}} \sum_{n'=0}^{N_\mathrm{s}-1} h[n', m; q] e^{-j2\pi d n'/N_\mathrm{s}}, \tag{5}$$

and the local scattering function is then obtained by

$$P[m, d; q] = |s[m, d; q]|^2, \tag{6}$$

where the Doppler domain has a resolution $\Delta\eta = 1/(\Delta t N_\mathrm{s})$. Please note, for each q^{th} local area, we obtained a value of the scattering function.

In addition, (6) is used in [19] to analyze the behavior of the local power delay profile $P_\tau[m; q]$, as well as the local Doppler spectral density $P_\eta[d; q]$. Both are defined by

$$P_\tau[m; q] = \frac{1}{N_\mathrm{s}} \sum_{i=-N_\mathrm{s}/2}^{N_\mathrm{s}/2-1} P[m, i; q], \tag{7}$$

and,

$$P_\eta[d; q] = \frac{1}{N_\mathrm{b}} \sum_{i=0}^{N_{\mathrm{b}-1}} P[i, d; q]. \tag{8}$$

The Doppler frequency in $P_\eta[d; q]$ varies from a positive value to a negative one, depending on the direction of the vehicle movement and the location of scatterers. Finally, an estimation of the scattering function in the wireless channel is carried out taking the sample mean of $P[m, d; q]$, averaging the Q independent samples of the scattering function as

$$\hat{P}[m, d] = \hat{\mathbb{E}}[P[m, d; q]] = \frac{1}{Q} \sum_{q=1}^{Q} P[m, d; q]. \tag{9}$$

This approach allows balancing the noise variance. Furthermore, $P[m, d]$ can significantly change within a single scenario due to the change of relative speed and the emergence of moving scatterers.

Relationships between the correlation functions, power spectral densities, and statistics of a WSSUS channel are calculated from the scattering function as shown in [21] and [22]. Fig. 2 shows a simplified diagram of these relationships, where $C_\tau[d']$ is the frequency correlation function, $C_\eta[m']$ is the time correlation function, $P_\tau[m]$ is the average power delay profile, and $P_\eta[d]$ is the average Doppler spectral density.

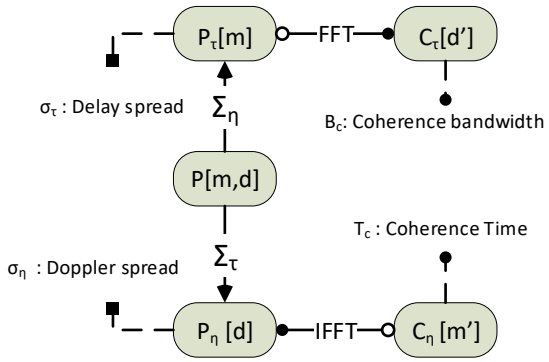

Fig. 2. Processing of the scattering function [23] in a WSSUS channel model.

Furthermore, the frequency and time selectivity of the channel can be derived from its channel statistics. While coherence bandwidth β_c and delay spread σ_τ are quantities which describe the dispersive nature of the channel, coherence time T_c and Doppler spread σ_η describe the time variation of the channel [24].

C. Tapped delay line model

If WSSUS is assumed, a TDL model is an efficient way to model (4) using both (7) and (9). The TDL model has been widely used to model the wideband impulse response as the sum of delayed multipath components [25]. It is based on statistical parameters, where each tap is associated with an amplitude coefficient a_i, a delay τ_i, and a Doppler spectrum P_{η_i} that determines how fast a_i changes over time.

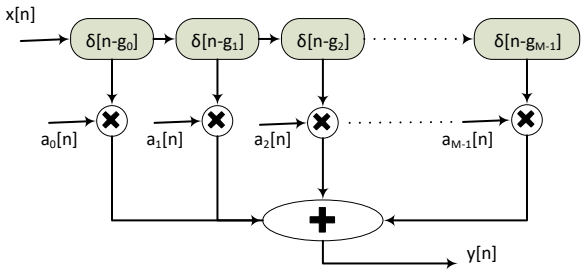

Fig. 3. Representation of a TDL model as a time-varying FIR filter.

Fig. 3 shows a simplified representation of the TDL model as a time-varying finite impulse response (FIR) filter, where $g_i = \lceil (\tau_i - \tau_{i-1})/\Delta\tau \rceil$ represents the relative discrete delay and $a_i[n]$ represents the complex channel gain which depends on the amplitude coefficient of the tap and its Doppler spectrum. In addition, the Doppler spectrum for each tap P_{η_i} in a TDL model can be obtained from $P[m, d]$. Then, the implementation of a TDL model requires the knowledge of the following parameters:

- Number of taps M
- Delay associated with each tap τ_i
- Magnitude associated with each tap a_i
- Doppler spectrum associated with each tap P_{η_i}
- Distribution of tap amplitudes
- Speed range, distance, and bandwidth considered

The procedure for estimating all listed parameters from $h[n, m]$ will be explained in detail in the next sections.

The TDL model only simulates the small-scale channel behavior which is due to multipath effect and mobility. The maximum Doppler frequency simulated in a TDL model depends on f_c which can cause frequency distortions in the received signal. Please note that the Doppler frequency and the channel coherence time are inversely proportional [16]. Hence, measured channels with different f_c have different channel statistics. Thus, f_c must be chosen according to the intended communication system. In the literature, we have found two T2T channel models valid for frequencies below 1 GHz [8], [11], so they are not valid to evaluate the behavior of any vehicular communication system which operates in the 5.9 GHz band or millimeter band.

D. Railway channel measurement campaign

In this paper, we develop a TDL model for T2T propagation scenarios based on a channel sounding measurement campaign carried out by the German Aerospace Center (DLR) within the scope of the Roll2Rail project. Settings of the T2T measurement campaign are listed in Table I and are explained in detail in [2]. The DLR channel sounder was used in single-input single-output (SISO) mode to measure $h[n, m]$ for different scenarios and maneuvers. The measurements were conducted on a 205 km long high speed railway (HSR) track between Naples and Rome. The trains were driving on parallel tracks for safety reasons.

TABLE I
SETTINGS OF DLR CHANNEL SOUNDER [2].

Parameters	Value
Central frequency f_c	5.2 GHz
Bandwidth W	120 MHz
Snapshot rate Δt	1.024 ms
EIRP	33 dB
Number of bins N_b	1537
Antenna type	omnidirectional
Antenna gain	6 dBi

EIRP = Effective Isotropic Radiated Power

1) Measurement scenarios: We analyze the following scenarios:

- Hilly Terrain: It is characterized by dense scatterers throughout the environment with objects distributed irregularly and non uniformly (Fig. 4a). Thus, the received signal will be subject to multipath fading. The LoS component can be even observed at large distances of 800 m as the railway track runs straight and no larger obstacles occur (please see Fig. 5). Also, long lasting multipath components can be received, which can provoke the dispersion in both delay and Doppler domains. In this scenario, both trains travel in the same direction in an approaching maneuver with a constant relative speed of 40 km/h.
- Railway Station: It is characterized by a dense network of railway infrastructure like platforms, buildings, other trains, overhead systems, and signaling systems as depicted in Fig. 4b. As a result, this scenario is rich of reflecting and scattering objects. Hence, low values of k-factor can be expected, although the LoS component is constantly observable. In this scenario, an approaching maneuver was carried out, where one train was standing on the platform and the other one decelerated from 50 km/h to 0 km/h.

In both scenarios, the overhead line system with the catenary and the supporting masts are kept in all environments and have a significant influence on the wireless propagation [26].

2) Considered T2T distances: The channel statistics for each considered scenario are analyzed in three segments as

- Short distance: 5 m to 100 m
- Medium distance: 400 m to 500 m
- Large distance: 800 m to 900 m

The subdivision in segments is motivated by the number of resolvable multipath components N_rm, which is correlated with the T2T distance. This effect can be seen in Fig. 5, where N_rm changes for the analyzed local areas. As a result, different dynamic ranges for the power are obtained for the local areas

(a) Hilly Terrain scenario

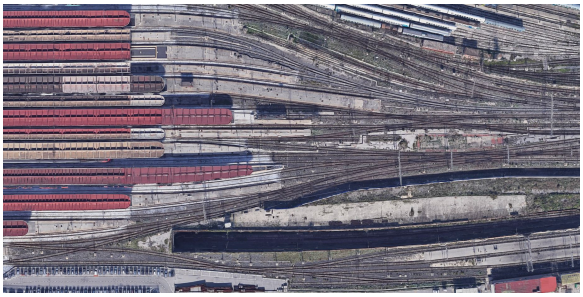

(b) Napoli Centrale Railway Station

Fig. 4. Considered scenarios in the DLR measurement campaign [26].

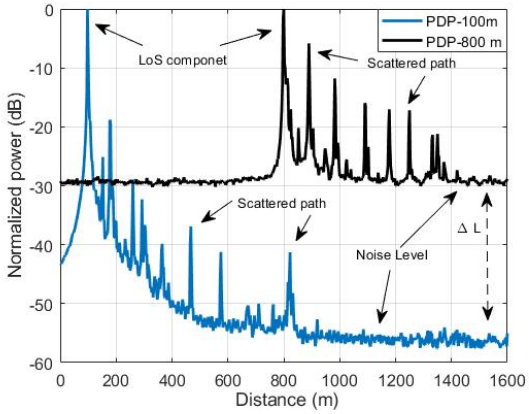

Fig. 5. Measured normalized power delay profile (PDP) for two local areas located at train-to-train distances of 100 m and 800 m. The distance axis is obtained by multiplying the delay with the speed of light.

based on a threshold β_{t}. Thus, a multipath component is resolvable when its normalized power is higher than β_{t}.

In addition, different noise levels are observed as a consequence of the normalization operation in Fig. 5. The power interval between them (ΔL) can be interpreted as the path loss that the transmitted signal suffers in $[r_1; r_2]$ interval. Then, $\Delta L \approx 10\gamma \log(r_1/r_2)$ can be obtained considering that the shadow fading is assumed to be a Gaussian distributed random variable with zero mean and variance σ^2. γ describes the path loss exponent, and r_1 and r_2 the average distances in two local areas (S_q and $S_{q'}$) in S. Using the path loss model shown in [26] for this scenario, where $\gamma = 3.1$, the result is $\Delta L \approx 28$ dB. This result matches well with what is observed in Fig. 5.

For future T2T applications, it is important also to know the statistics of the wireless channel at certain T2T distances. For instance, in the use case of smart train composition coupling, the T2T distance must be kept within a certain distance range when both trains become virtually coupled [12].

III. T2T Tapped Delay Line Models

Using the stored data in the DLR measurement campaign, the parameters of the TDL model, that were presented in Section II-C, will be estimated in this section. The used data reflects the propagation conditions in a realistic T2T scenario.

A. Computation of TDL model parameters

In this subsection, the methodology to derive the channel parameters is presented in detail, which allows to simulate a measured T2T wireless channel using a TDL model.

1) Delay and power values in TDL model: The TDL channel model consists of M taps with a resolution in delay equal to $R_\tau = 1/W_{\mathrm{p}}$, where W_{p} is the bandwidth of the intended communication system. The taps are characterized by a delay τ_i and a magnitude a_i ($i = 1, ..., M$). Their estimates are based on the local power delay profile $P_\tau[m; q]$ which can be related to $h[n', m; q]$ substituting (5) and (6) in (7) as

$$P_\tau[m; q] = \frac{1}{N_{\mathrm{s}}} \sum_{n'=0}^{N_{\mathrm{s}}-1} |h[n', m; q]|^2, \tag{10}$$

where the square magnitude of N_{s} impulse responses in the q^{th} local area are averaged [27]. By taking the average power, we result in the small-scale fading characteristics of the local area.

In the following, the dynamic range in the interval $[i_q; i_q + bM]$ is established for each $P_\tau[m; q]$ based on a threshold β_{t}, where the part of the power density below the threshold is set to zero. Also, M is chosen based on both β_{t} and R_τ similar to [28], where β_{t} is used to eliminate noise which could be mistaken as a multipath component. The dynamic range is divided into M groups with $b = R_\tau/\Delta\tau$ samples. After that, the first sample of each group is indexed by m_i, where m_1 is the index of the first nonzero sample after applying the threshold [29]. Next, the average delay for the i^{th} tap and q^{th} local area is calculated using the first moment of $P_\tau[m; q]$ as

$$\tau_{i;q} = \frac{\sum_{m'=m_i}^{m_i+b-1} m' \Delta\tau P_\tau[m'; q]}{\sum_{m'=m_i}^{m_i+b-1} P_\tau[m'; q]}. \tag{11}$$

From (11), Q independent samples of τ_i are obtained for each tap (one sample for each local area). An estimate of the expected delay for each tap is achieved taking the average over $\tau_{i;q}$ as

$$\hat{\tau}_i = \hat{\mathbb{E}}[\tau_{i;q}] = \frac{1}{Q} \sum_{q=1}^{Q} \tau_{i;q}. \tag{12}$$

Please note that the aforementioned τ_i values are generally not equidistant in delay. Also, the average power in each tap at S_q is calculated as

$$a_{i;q} = \frac{1}{b} \sum_{m'=m_i}^{m_i+b-1} P_\tau[m'; q], \tag{13}$$

and finally $\hat{a}_i = \hat{\mathbb{E}}[a_{i;q}]$. The authors in [29] and [30] used (11) and (13) to develop a TDL model based on mobile radio propagation measurements. However, these models were not tested with a communication system to validate its performance.

Also, applying the dynamic range in $h[n', m; q]$, N_s complex amplitude samples for each tap i are obtained in a local area q by averaging the amplitudes in the delay domain as

$$r_{n',i;q} = \frac{1}{b} \sum_{m'=m_i}^{m_i+b-1} h[n', m'; q], \tag{14}$$

which are grouped into a three-dimensional complex matrix with $N_\mathrm{s} \times M \times Q$ elements. This matrix will be used to estimate the Rice factor for each tap k_i in the next subsection.

2) Envelope amplitude distribution: The amplitude distribution of the complex channel tap gain $r_{n',i;q}$ is investigated in order to determine the distribution of its envelope. This gain can be modelled by a Gaussian random variable, and consists of a fixed component plus a zero-mean fluctuating component [31]. When there is a dominant or LoS component, a Rician distribution is expected for the envelope of the complex channel tap gain R. The Rician distribution is characterized by the k-factor, which indicates the severity of the fading in the channel.

In this paper, the k-factor is estimated using the maximum likelihood method from [32], optimizing the likelihood numerically in the following equation

$$\frac{1}{1+k} + \frac{1+2k}{N_\mathrm{s}\sqrt{k(1+k)}} \sum_{n=1}^{N_\mathrm{s}} \frac{y_n I_1(y'_n)}{I_0(y'_n)} = 1 + \frac{1}{N_\mathrm{s}} \sum_{n=1}^{N_\mathrm{s}} y_n^2, \tag{15}$$

being $y'_n = 2y_n\sqrt{k(k+1)}$, y_n the normalized envelope, and $I_m(x)$ the m^{th} order modified Bessel function.

The procedure for estimating $k_{i;q}$ (k-factor of i^{th} tap at a local area S_q) is summarized as follows

- For each tap i in a S_q, N_s independent samples of $r_{n',i;q}$ are taken $(r_{0,i;q}, r_{1,i;q}, \cdots, r_{N_\mathrm{s}-1,i;q})$, and its envelope $R_{n'}$ is calculated.
- The envelope is normalized with respect to the total mean power, i.e. normalized envelope $y_{n'} = R_{n'}/\hat{\mathbb{E}}[R^2_{n'}]$.
- Finally, the roots of (15) are calculated to obtain $k_{i;q}$.

Having obtained $k_{i;q}$, the k-factor for each tap i is estimated by the sample mean $\hat{k}_i = \hat{\mathbb{E}}[k_{i;q}]$. It will be used to characterize the amplitude distribution of the envelope.

3) Doppler spectrum per Tap: The variation of $h[n, m]$ determines the Doppler spectrum of each resolvable tap. For implementing these Doppler spectra into the TDL channel model only the shape and the distribution are required to generate a channel representation with similar statistics and Doppler behaviour like the measured channel [29]. The Doppler spectrum for the i^{th} tap can be estimated using the scattering function by

$$\hat{P}_{\eta_i}[d] = \frac{1}{b} \sum_{n=0}^{b-1} P[m_{i,n}, d], \tag{16}$$

where $m_{i,n} = m_\mathrm{los} + (i-1)b + n$, and m_los is the average delay of the LoS component which can be obtained from $P_\tau[m]$. (16) allows to obtain a Doppler spectrum for each tap, which might have different statistical distributions [33].

Another approach is to use the same Doppler spectral shape for each tap. Given that, the Doppler spectrum for each tap i is estimated as a constant, and defined by

$$\hat{P}_{\eta_i}[d] = P_\eta[d], \tag{17}$$

where $P_\eta[d]$ was defined in Section II-B. This choice simplifies the model and reduces its complexity. Then, the implementation of $P_{\eta_i}[d]$ into the TDL model is carried out using two operation modes which are named: DSP0 and DSP1. The DSP0 mode uses a Doppler spectrum approach by applying (17), while the DSP1 mode uses the Doppler spectrum approach based on $P[m, d]$ as defined in (16). Hence, we will validate in Section IV-C how well these modes performs compared to measured channel impulse responses.

B. Results and analysis of the proposed TDL channel models

In this subsection, the procedure shown in the previous subsections is applied to six different propagation channels and the obtained results are shown and analyzed. The considered channels are named from MD1 to MD6, which differ in the propagation scenarios (Hilly Terrain and Railway Station) and the considered T2T distances (short, medium and large).

1) Doppler-delay spectrum: The Hilly Terrain scenario and short distances are considered in the MD1 channel model. Fig. 6a shows the normalized Doppler-delay spectrum for this scenario, where the delay and the Doppler frequency can be related to the power of any received multipath component. Given that the relative speed Δv is constant, we can clearly identify the Doppler frequency η_los of the LoS component and the maximum Doppler frequency η_max of the reflecting and scattering obstacles located along the track. Using (2) with $\alpha = 0$, these Doppler frequencies can be calculated by

$$\eta_\mathrm{los,max} = \frac{(v_\mathrm{t} \mp v_\mathrm{r}) f_\mathrm{c}}{c},$$

where $v_\mathrm{t} = 50$ km/h and $v_\mathrm{r} = 10$ km/h, as shown in Fig. 1, represent the speed of the rear and front trains, respectively. Then, the LoS component is located at $\eta_\mathrm{los} = 193$ Hz and it describes a red vertical line in the spectrum. Positive η_los indicates that the trains are approaching. In contrast, the scattering components, with less power, exhibit a maximum Doppler of $\eta_\mathrm{max} = 289$ Hz.

Please note, that when the angle of arrival α of the scattered path varies from 0 rad to π rad, the scattering Doppler frequency can become negative and takes a minimum value of $-\eta_\mathrm{max}$. Moreover, the delay of the LoS component varies from 341 ns to 25 ns, which corresponds with the analyzed interval (100 m to 5 m). In addition, when the T2T distance

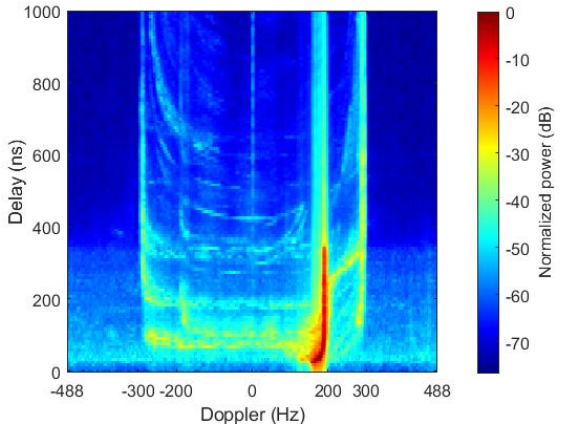

(a) Normalized Doppler-delay spectrum $\hat{P}[m, d]$

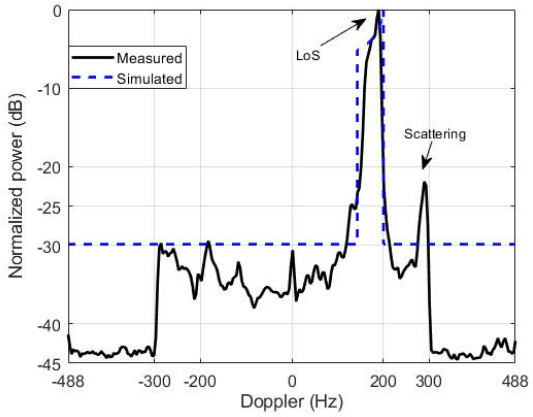

(b) Normalized average Doppler spectrum $P_\eta[d]$

Fig. 6. MD1 channel model is modelled in a Hilly Terrain scenario.

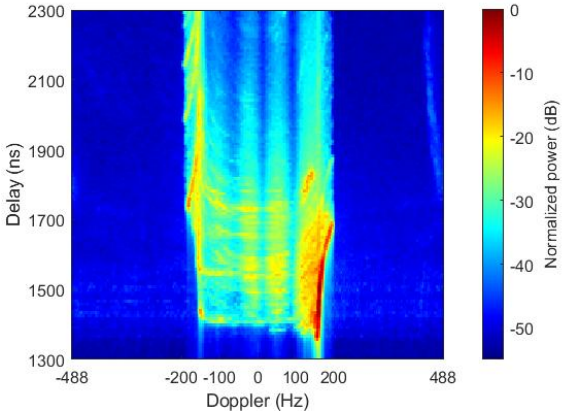

(a) Normalized Doppler-delay spectrum $\hat{P}[m, d]$

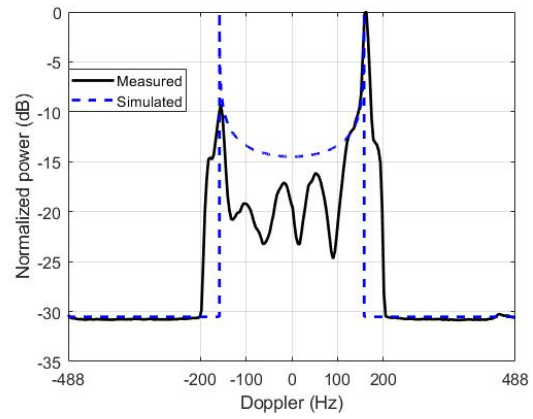

(b) Normalized average Doppler spectrum $P_\eta[d]$

Fig. 7. MD5 channel model is modelled in a Railway Station scenario. The part of $\hat{P}[m, d]$ below 1 300 ns is not shown as it corresponds to noise.

gets close to 15 m, both trains are about to cross and η_{los} starts to decrease since its angle of arrival begins to vary from 0 rad to $\pi/2$ rad. Moreover, the number of multipath components increases as reflections from the metal structure of the train and multipath components with similar power to as the LoS component can be observed. These effects can be seen in Fig. 6a for delays below 50 ns.

The average Doppler spectrum is computed for this scenario and shown in Fig. 6b, where the Doppler frequencies $\eta_{\text{los,max}}$ can be easily determined since they reach a peak power. The power of the LoS component exceeds the maximum multipath component by more than 20 dB. As it can be observed, the shape of the Doppler spectrum matches a "Rice" type. The "Rice" spectrum is expected to occur in scenarios where the LoS component is dominant [34]. In addition, the simulated Doppler spectrum is shown in this figure as dashed blue line. The analytical expressions of all simulated Doppler spectra and the used model selection criteria are presented in Appendix A.

Different propagation conditions can be applied to a communications system if we select the MD4 channel model, where the Railway Station scenario and medium distance are considered. In this scenario, $v_{\text{r}} = 0$ and v_{t} varies from 41 km/h to 36 km/h. Since $v_{\text{r}} = 0$, $\eta_{\text{los,max}}$ can overlap and scattering components can be observed close to $\pm\eta_{\text{los}}$. Fig. 7a shows the normalized Doppler-delay spectrum for this scenario. The maximum Doppler component is determined by the LoS component, which slightly varies from 197 Hz to 174 Hz (semi-curved red line) as Δv is not constant. In addition, some scattering Doppler frequencies are densely located close to η_{los}. This finding indicates that this scenario is very rich in reflecting obstacles and a high rate of scatterers is expected.

The delay of the LoS component varies from 1 692 ns to 1 350 ns, which corresponds with the analyzed interval (500 m to 400 m). Also, if the delay is constant, for instance 1 550 ns, there are scatterers with significant power around -20 dB, whose Doppler vary in the $[-\eta_{\text{los}}; \eta_{\text{los}}]$ interval. In the spectrum, they can describe a horizontal line and it might be identified as reflections stemming from the catenaries. Then, some horizontal lines are seen in $\hat{P}[m, d]$ in both scenarios (see Fig. 6a and Fig. 7a), since the catenaries are periodically located long the track.

Fig. 7b shows the average Doppler spectrum for this sce-

TABLE II
PROPOSED DOPPLER SPECTRUM FOR EACH TAP.

Mode	Taps	MD1			MD2			MD3			MD4			MD5			MD6		
		η_{d_1}	η_{d_2}	**shape**	η_{d_1}	η_{d_2}	**shape**	η_{d_1}	η_{d_2}	**shape**	η_{d_1}	η_{d_2}	**shape**	η_{d_1}	η_{d_2}	**shape**	η_{d_1}	η_{d_2}	**shape**
DSP0	1$\rightarrow M$	143	200	Rice	178	216	Rice	280	312	Rice	75	-	Flat	158	-	Jakes	266	-	Jakes
DSP1	1	116	201	Rice	174	271	Rice	166	220	Rice	6	36	Rice	120	170	Rice	185	277	Rice
	2	147	208	Rice	174	216	Rice	181	224	Rice	31	-	Jakes	109	174	Rice	32	281	Rice
	3	170	224	Rice	174	212	Rice	174	312	Rice	73	-	Jakes	166	-	Jakes	-78	277	Rice
	4	155	204	Rice	170	212	Rice	185	250	Rice	79	-	Flat	190	-	Jakes	262	-	Jakes
	5	304	-	Jakes	170	304	Rice	166	315	Rice	78	-	Flat	174	-	Jakes	266	-	Jakes
	6	304	-	Jakes	292	-	Jakes	189	312	Rice	76	-	flat	151	-	Jakes	269	-	Jakes
	7	304	-	Jakes	250	304	Rice	185	315	Rice	76	-	Flat	157	-	Jakes	262	-	Jakes
	8				289	-	Jakes	269	315	Rice	76	-	Flat	162	-	Jakes	262	-	Jakes
	9				289	-	Jakes	266	315	Rice	74	-	Flat	158	-	Jakes	266	-	Jakes
	10				289	-	Jakes	277	315	Rice	74	-	Flat	158	-	Jakes	269	-	Jakes
	11				292	-	Jakes	266	315	Rice	74	-	Flat	166	-	Jakes	262	-	Jakes
	12				266	-	Jakes	281	315	Rice				158	-	Jakes	266	-	Jakes
	13							273	315	Rice				158	-	Jakes	262	-	Jakes
	14							289	315	Rice				158	-	Jakes	266	-	Jakes
	15							285	315	Rice				158	-	Jakes	266	-	Jakes
	16							281	315	Rice				158	-	Jakes	266	-	Jakes

η_{d_1} and η_{d_2} are expressed in Hertz (Hz) which define the modelled Doppler spectra (see Appendix A)

TABLE III
PARAMETERS OF THE PROPOSED CHANNEL MODELS: POWER, DELAY AND k-FACTOR.

Taps	MD1			MD2			MD3			MD4			MD5			MD6		
	$\hat{a}_i$ (dB)	$\hat{\tau}_i$ (ns)	$\hat{k}_i$ (dB)	$\hat{a}_i$ (dB)	$\hat{\tau}_i$ (ns)	$\hat{k}_i$ (dB)	$\hat{a}_i$ (dB)	$\hat{\tau}_i$ (ns)	$\hat{k}_i$ (dB)	$\hat{a}_i$ (dB)	$\hat{\tau}_i$ (ns)	$\hat{k}_i$ (dB)	$\hat{a}_i$ (dB)	$\hat{\tau}_i$ (ns)	$\hat{k}_i$ (dB)	$\hat{a}_i$ (dB)	$\hat{\tau}_i$ (ns)	$\hat{k}_i$ (dB)
1	0.0	0	12.5	0.0	0	9.0	0.0	0	6.0	0.0	0	6.0	0.0	0	4.0	0.0	0	4.0
2	-17.3	58	-6.0	-16.3	110	-4.0	-11.0	104	-4.0	-16.0	94	-5.0	-8.1	106	-8.5	-7.4	100	-9.0
3	-21.5	178	0.5	-20.3	204	-0.5	-14.4	200	-8.0	-18.5	194	1.0	-11.6	200	-7.5	-10.2	196	-7.0
4	-24.8	260	0.0	-18.0	320	0.0	-13.1	320	-2.0	-21.6	298	0.5	-14.2	308	-7.0	-12.1	304	-7.0
5	-30.2	380	-4.5	-18.8	410	-3.5	-13.2	406	-2.0	-21.7	400	0.5	-15.7	408	-7.0	-12.5	402	-5.0
6	-28.4	460	-4.0	-23.0	522	-5.5	-17.4	510	-9.5	-22.9	496	-2.0	-15.7	514	-3.5	-13.6	504	-4.5
7	-29.9	538	-3.0	-18.8	610	1.0	-14.7	620	-4.0	-25.3	598	-2.0	-16.4	608	-1.5	-15.0	604	-2.5
8				-24.1	722	-7.0	-11.3	708	2.5	-25.2	688	0.0	-18.2	706	-3.0	-16.0	704	-9.0
9				-20.9	836	-4.5	-17.3	806	-8.0	-27.1	798	-3.5	-19.2	808	-3.0	-16.3	804	-5.5
10				-23.9	914	-2.5	-19.3	912	-16.0	-27.0	902	-2.5	-20.2	908	-2.5	-16.5	904	-2.0
11				-23.9	1 024	-10.0	-15.1	1 014	-5.0	-21.1	1 008	-0.5	-20.7	1 006	-5.0	-17.2	1 002	-4.5
12				-19.7	1 106	-2.5	-16.2	1 104	-1.5				-21.5	1 110	-4.5	-18.1	1 098	-4.5
13							-19.0	1 212	-12.5				-22.8	1 214	-3.0	-18.4	1 200	-5.0
14							-15.4	1 312	-5.5				-21.9	1 310	-4.5	-18.5	1 302	-8.5
15							-17.3	1 404	-6.0				-20.3	1 414	-3.5	-18.2	1 404	-3.0
16							-17.5	1 512	-12.0				-22.5	1 502	-3.0	-19.4	1 500	-7.5

nario, where scatterers with both positive and negative Doppler frequencies can be observed. Also, two peak powers are located at a Doppler frequency of ± 158 Hz and different powers. The difference in power may be attributed to both the non-uniform distribution of the scatterers in the scenario and the LoS component that appears with positive Doppler, which can be verified in Fig. 7a. In this scenario, the shape of the Doppler spectrum is identified as "Jakes" type.

2) Doppler spectrum per tap: The shape of Doppler spectra in all considered scenarios are listed in Table II, where the η_{d_1} and η_{d_2} frequencies, which are expressed in Hz, specify the spectrum (see Appendix A). Using this table, the modelled Doppler spectra can be implemented in the TDL model using the DSP0 and DSP1 modes, as explained in Section III-A3. In addition, it is observed that in all analyzed scenarios, the first tap follows a "Rice" type Doppler spectrum, which indicates that the LoS component is always dominant even though large distances are considered. Another finding is that the taps can exhibit different spectrum types for the same scenario.

3) Amplitude, delay and k-factor per tap: Table III shows the power, delay, and k-factor for each resolvable tap in each considered model. The accuracy of estimated parameters were chosen using an confidence interval of 95 %, where an accuracy of one digit after the decimal point for $\hat{a}_i$, 2 ns for $\hat{\tau}_i$ and 0.5 dB for $\hat{k}_i$ were used. Please see Appendix B where the confidence intervals for the MD1 and MD5 proposed TDL models are provided.

As expected, the results always show that the first tap exhibits higher k-factor than the rest. As a consequence, the amplitude of the first tap is simulated following a Rician distribution, while the other ones follow a Rayleigh distribution. The maximum delay $\hat{\tau}_{\max} = \hat{\tau}_{\mathrm{M}} - \hat{\tau}_1$ is higher than 1 μs except in the MD1 model, where $\tau_{\max}$ is equal to 538 ns. The maximum number of resolvable taps is equal to 16 in the MD3, MD5 and MD6 models. Thus, the proposed channel models can be emulated using a channel emulator which allows to carry out a system-level simulation [35].

Furthermore, we consider that the differences among the three proposed channel models (MD4, MD5 and MD6) in Railway Station are caused by two variables: T2T distance and relative speed. While the T2T distance is correlated with the number of multipath components (see Section II-D2) which affects the obtained value M and the relative power of each tap, Δv determines the free variables (η_{d1} and η_{d2}) of the shape of P_{η_i}. On the other hand, these differences in Hilly Terrain would be only caused by the T2T distance since Δv is constant for the three considered propagation scenarios.

4) Statistic of the proposed channel model: Channel statistics change considerably from one environment to another, over time and along T2T distance [14]. We are interested in investigating their averaged values and its dependence on the T2T distance. They are obtained based on $P[m, n]$ by using

TABLE IV
CHANNEL STATISTICS OF THE ANALYZED WIRELESS CHANNELS.

Model	**Scenario**	**Distance (m)**	σ_τ**(ns)**	$\bar{\tau}$**(ns)**	σ_η**(Hz)**	$\bar{\eta}$ **(Hz)**	T_c **(ms)**	B_c **(MHz)**	$\hat{k}_1$ **(dB)**	M	β_t **(dB)**	t_s **(ms)**	N_h	Δv **(km/h)**
MD1	HT	5 to 100	84	96	37	178	74.8	4.87	12.5	7	30	207.7	8 777	40
MD2	HT	400 to 500	192	1 522	107	177	59.7	1.94	9.0	12	20	207.7	8 777	40
MD3	HT	800 to 900	820	2 974	218	137	46.2	1.58	6.0	16	20	207.7	8 777	40
MD4	RS	5 to 100	86	106	18	27	77.2	5.57	6.0	11	25	756.5	39 000	5
MD5	RS	400 to 500	290	1 600	126	96	63.0	1.81	4.0	16	20	216.1	10 250	38
MD6	RS	800 to 900	572	2 940	233	92	26.2	1.34	4.0	16	20	167.5	6 408	49

HT = Hilly Terrain; RS = Railway Station; N_h = total number of used impulse responses; $\bar{\tau}$ = mean delay; $\bar{\eta}$ = mean Doppler

the diagram shown in Fig. 2. The obtained statistics of the analyzed channels are shown in Table IV. It is observed that both delay spread σ_τ and Doppler spread σ_η are correlated with the T2T distance. For instance, when we move from short distance (MD1) to medium distance (MD2), σ_τ increases from 84 ns to 192 ns, while σ_η increases from 37 Hz to 107 Hz.

These results indicate that the channel dispersion in time-frequency domains increases with the distance, which is reasonable to expect since the number of resolvable multipath components increases with distance (see Fig. 5). Please note that the T2T distance determines the geometric relation between the trains and the environment, thereby this relation would be reflected in the channel statistics. The distance-dependent effect is also seen in $\hat{k}_1$, which relates the power of the LoS component and the scattered paths. Thus, $\hat{k}_1$ varies from 12.5 dB to 6.0 dB when short (MD1) and large (MD3) distances are considered in Hilly Terrain.

These finding match with the results shown in [15] where the behaviour of the k_1, σ_τ, and σ_η parameters with respect to T2T distance are shown. In addition, the coherence time T_c and the coherence bandwidth B_c are also shown in Table IV, being both dependent on the distance too. The knowledge of the wireless channel statistics is very important in order to optimize the design of any communication system. For instance, σ_τ determines the length of cyclic prefix in orthogonal frequency division multiplexing (OFDM) systems [36], while σ_η determines the separation of midambles in 802.11bd.

IV. ANALYSIS AND VALIDATION OF THE PROPOSED CHANNEL MODELS

In this section, the novel 802.11bd protocol and measured channel impulse response (CIR) are used to validate the proposed TDL channel models. A validation framework is proposed and the obtained results are shown and analyzed. 802.11bd has been chosen for the validation, since the T2T communication is one of its use cases [1].

A. 802.11bd vehicular protocol

In the last decade, vehicular communications have been supported by the well-known 802.11p protocol, which enables intelligent transport systems (ITS) that support critical and non-critical applications. Nowadays, its evolution, named 802.11bd, is being standardized by the IEEE standardization group (TGbd), whose new use cases have been defined in [37].

802.11bd will introduce novel processing techniques and keep the constrains of backward compatibility. An 802.11bd specification framework was presented in [3], where the following setting candidates were tested by TGbd:

- 10/20 MHz bandwidth
- Channel tracking based on midamble
- Low density parity check (LDPC) coding
- 256QAM modulation
- Retransmissions
- Multiple-input multiple-output (MIMO) techniques
- Dual constellation modulation (DCM)

The new protocol increases the numbers of active carriers to 56 with a mandatory bandwidth of 10 MHz. It uses the LDPC coding to increase robustness against channel impairments, although binary convolutional coding (BCC) is still supported for backwards compatibility with 802.11p. Further, midambles are used to update the channel response estimation by periodically inserting training symbols into the sequence of data OFDM symbols, tracking the wireless channel in this way.

In addition, the transmission range is increased using diversity techniques such as DCM. While, the MIMO techniques, the 256QAM modulation, and 20 MHz bandwidth allow to double the transmission rate. As a result, the implementation of new use cases, which demands higher data rates, is possible, e.i. sensor sharing, automated driving assistance among others. For the validation of the proposed TDL channel models, an 802.11bd compliant physical layer has been implemented in MATLAB based on [3].

Synchronization in the 802.11bd receptor is carried out using training symbols in the same way as in [38]. The receiver exploits the periodicity of the short training symbols by calculating the autocorrelation coefficient of the received signal. Then, this coefficient is compared with a threshold to decide if the packet is detected or not. After that, the alignment symbol is carried out using a matched filter to cross-correlate the sample stream with the known pattern of the long training

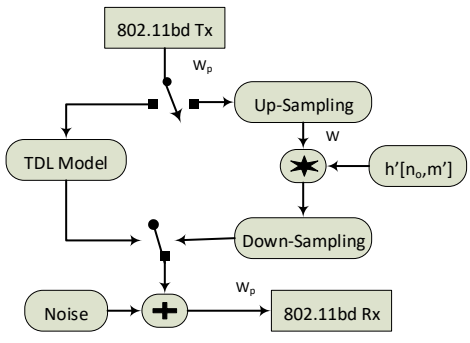

Fig. 8. Diagram of the validation framework of the proposed channel models.

symbols. Finally, frequency offset is estimated and corrected. To test the synchronization, we add a number of random null samples at the beginning and end of each frame.

B. 802.11bd performance based validation

In order to evaluate the performance and the accuracy of the TDL models proposed in the previous section, a base-band validation framework showing in Fig. 8 is implemented through simulating a single link between a transmitter and receiver for two different options: using the measured channel impulse response $h[n, m]$ or the TDL channel model. Then, the performance results for both validation options are compared and analyzed using packet error rate (PER) versus E_{b}/N_0, where E_{b} denotes the energy per bit and N_0 the noise power spectral density which is defined as in [39].

Using the reference validation option (first option) in Fig. 8, the switch will move to the right. Firstly, the 802.11bd signal has to be up-sampled as its bandwidth W_{p} is usually lower than the measurement bandwidth W. Secondly, the convolution process is carried out to emulate the impairments of the wireless channel. On the convolution, the normalized impulse response $h'[n_o, m']$, with discrete time index n_o, is obtained by taking the samples within the dynamic range and normalizing them as

$$h'[n_o, m'] = \frac{h[n_o, i_p + m']}{\sum_{i=0}^{Mb-1} |h[n_o, i_p + i]|^2}$$
$$p = \lceil n_o/Q \rceil,$$
$$m' \in [0; Mb - 1]. \quad (18)$$

Please note that $h[n_o, m']$ is a sample of the CIR from stored measurement data, which indicates that the same data is used for fitting and testing of the proposed model. This choice was made due to the limited amount of stored data in the analyzed scenarios. This limitation is due to the limited availability of measurement time and equipment for railway measurements. Consequently, the validation model considers only the fitting accuracy and it does take into account the prediction accuracy.

The total number of measured impulse response N_h in each scenario is shown in Table IV.

The dynamic range is the same as the one applied in Section III-A and contains the significant energy of $h[n, m]$, smoothing in this way the noise. The normalization process in (18) removes the large-scale fading effect and its dependence with distance. Finally, the convolved output is downsampled. After adding the noise, it is processed at the receiver.

For the second option, the proposed TDL channel models are used to implement a Rician channel whose parameters are chosen from Table II and III, according to chosen TDL model. Please note, the Doppler spectrum $\hat{P}_{\eta i}[d]$ can be simulated in the Rician model in two different modes: DSP0 or DSP1, as was explained in Section III-A3. Then, noise is added and the signal is processed at the receiver.

C. Simulation results

Using the diagram in Fig. 8, the performance results of 802.11bd are estimated for each proposed validation option. Next, the PER performance of 802.11bd and 802.11p are compared using the MD1 channel model at different MCS. The simulation parameters are shown in Table V where the packet size is set to 400 byte.

TABLE V
SIMULATION PARAMETERS.

Parameters	802.11bd	802.11p
Bandwidth W_{p} (MHz)	10	10
Data carriers	52	48
Modulation order	2,4,16,64,256	2,4,16,64
Coding rate R_{c}	1/2,2/3,3/4	1/2, 2/3
Type coder	LDPC	BCC
Channel estimation	Midamble	Least square
Midamble rate	4	-
Payload (byte)	400	400
Simulated packets	40000	40000

Fig. 9a shows how the performance of 802.11bd is degraded when the T2T distance is increased in Hilly Terrain by changing the channel model. For instance, there are 5 dB of penalty when switching the channel model from MD1 to MD2 and $\mathrm{PER} = 10^{-2}$. The QPSK modulation and 1/2 coding rate

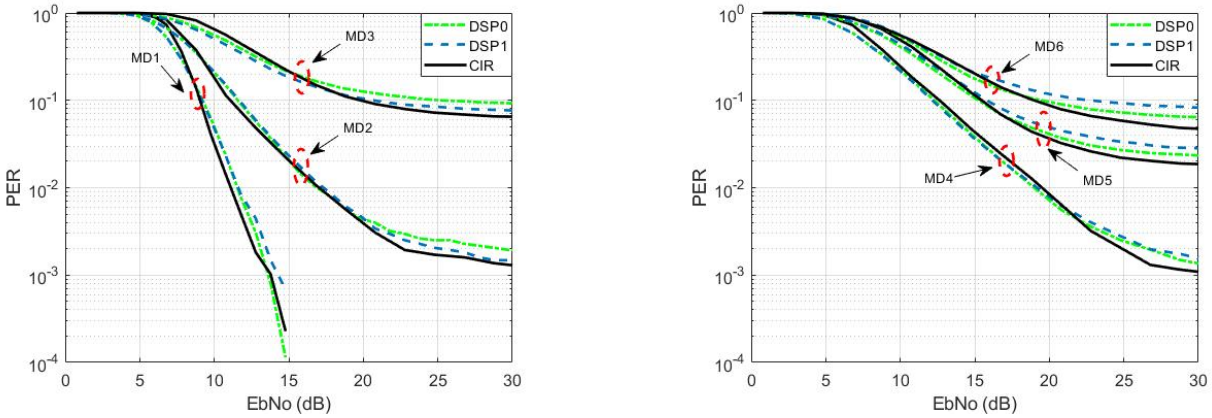

(a) Hilly Terrain scenario

(b) Railway Station scenario

Fig. 9. Validation results of the proposed channel models based on performance of 80211.bd using QPSK-1/2 at different T2T distances.

(QPSK-1/2) are used in this test. For any considered channel model, significant differences are hardly observed between the two options of simulated Doppler spectra (DSP0 and DSP1 modes). In both cases, the obtained performances match well. Finally, the proposed channel models (MD1, MD2 and MD3) degrade performance of 802.11bd in a similar way as in the case of using the measured channel impulse response (CIR). For instance, choosing $E_\mathrm{b}/N_0 = 25$ dB, a $\mathrm{PER} = 2.0 \cdot 10^{-3}$ ($2.5 \cdot 10^{-3}$) is reached through MD2 in the DSP1 (DSP0) mode while a $\mathrm{PER} = 1.8 \cdot 10^{-3}$ is reached if CIR is used.

Similar findings are obtained when the MD4, MD5 and MD6 channel models are tested, whose results are shown in Fig. 9b. Also, we can verify that Railway Station scenario is more demanding than Hilly Terrain scenario. For instance, to reach a $\mathrm{PER} = 10^{-2}$ at short distances, an E_b/N_0 of 11 dB is necessary for the MD1 model, while an E_b/N_0 of 19 dB is necessary for the MD4 model.

Also, an error floor close to 10 % of packect loss is observed for the MD3 and MD6 channel models. This effect can be caused by orthogonality loss of subcarriers in OFDM modulation due to both timing and channel estimation errors. As a result, inter-symbol interference degrades system performance. Although, the transmission of error-free packets is possible for the MD1 model, a low error floor is still seen for the MD2 and MD4 channel models.

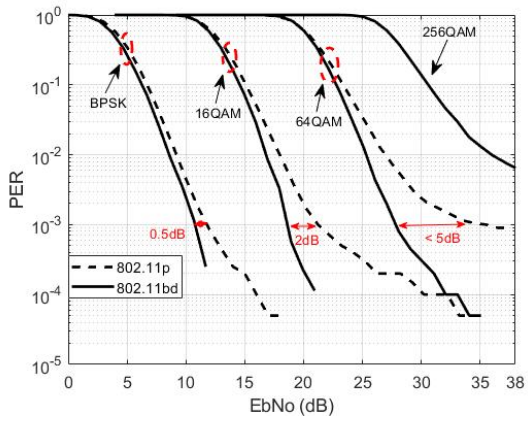

Fig. 10. Comparison between 802.11p and 802.11bd using the MD1 model (DSP0). The BPSK, 16QAM, 64QAM, and 256QAM modulations are combined with a coding rate of 1/2, 1/2, 2/3, and 3/4 respectively.

The performance results of 802.11p and 802.11bd for different MCS are shown in Fig. 10. The results reveal that using 16QAM-1/2 scheme and a target $\mathrm{PER} = 10^{-3}$, a performance gain of 2 dB in E_b/N_0 is obtained when 802.11bd is used instead of 802.11p. Also, 802.11bd achieves a gain of 0.5 dB and 5 dB for BPSK-1/2 and 64QAM-2/3 schemes, respectively. These results match with the ones shown in [40], where a gain from 1 dB to 3 dB was obtained by 802.11bd using other channel models. Finally, the behavior of 802.11bd using a higher order modulation (256QAM) is shown in this figure too, where a $\mathrm{PER} < 10^{-2}$ is obtained for $E_\mathrm{b}/N_0 > 36$ dB. This modulation is only available for 802.11bd which is used with $R_\mathrm{c} = 3/4$.

D. Work in progress and future work

Six TDL channel models have been proposed and validated for two T2T railway scenarios with trains moving with relative speeds up to 50 km/h. These speeds were used due to limitations on the measurement site and the channel sounder. In reality, although the trains could drive faster than 300 km/h, their relative speed $\Delta v'$ could be in the considered relative speed Δv range in this article. Given that, what would happen with the parameters of the proposed TDL models if other Δv and driving maneuvers are considered? This last question is another research gap in T2T communications, where new studies must be carried out.

In addition, a measurement campaign was carried out in [41] for different relative speeds in a T2I scenario. The results show that the measured PDP for $\Delta v = 100$ km/h behave similar to the measured PDP for $\Delta v = 200$ km/h in the same scenario. Also, the T2T communication based on TETRA was analyzed in [13], where no evidence was found of a possible influence of Δv on the message error rate. Based on the shown results in these articles, the following ideas arise for future work:

- The average power delay profile $P_\tau[m]$ does not change when Δv changes since it only depends on the geometry of the scenario. As a result, the stochastic channel parameters shown in Table III should remain valid.
- The average Doppler spectral density $P_\eta[d]$ is spread or compressed when Δv changes since Doppler frequency depends on Δv as was shown in (2). As a consequence, the channel parameters (η_{d_1} and η_{d_2}) shown in Table II should be scaled by a constant $C_\mathrm{d} = \Delta v'/\Delta v$.
- The channel statistics shown in Table IV should not change except $\bar{\eta}$, σ_η and T_c when Δv changes.

Therefore, measurements with different measurement settings e.g. higher velocities, higher bandwidth or MIMO setups would be of high interest. Additional parameters could be provided by a train-to-train geometry based stochastic channel model (T2T GSCM) where different velocities and various maneuvers could be considered in different environments. In a next step we will derive a T2T GSCM for different railway environments.

V. Conclusion

Modelling the wireless channel is one of the most difficult and relevant tasks of radio system design. In this paper, we have proposed six tapped delay line models for train-to-train communications. The Hilly Terrain and Railway Station scenarios are covered for large, medium, and short distances. The results indicate that the simulated channel using any of the proposed models is correlated with the measurements carried out with the DLR channel sounder, since both channels degrade the 802.11bd performance in a similar way. The proposed TDL models can be modelled using a maximum tap number of 16, and hence can be implemented in any modern channel emulator. Furthermore, the maximum delay is higher than 1 μs except for the MD1 model, whose maximum delay is 538 ns.

It is observed that the stochastic channel parameters are time variant and T2T distance dependent. For instance, delay spread

σ_τ varies from 84 ns to 820 ns when short or large distances are considered in Hily Terrain. Also, the analysis of Doppler-delay spectrum reveals that the Railway Station scenario is densely covered with reflector obstacles, which deteriorates the propagation conditions. The DSP0 and DSP1 modes, which describe how the Doppler spectrum is simulated, cause only small differences in the 802.11bd performance although the DSP0 mode is much simpler to implement. Finally, 802.11bd achieves a performance gain over 802.11p from 0.5 dB to 5 dB at a PER of 10^{-3} depending on the used modulation and coding scheme.

APPENDIX A
SIMULATED DOPPLER SPECTRUM

Three types of Doppler spectra are observed in the considered scenarios: "Jakes", "Rice" and "Flat". These spectra are defined by η_{d_1} and η_{d_2}, and form a pool of models based on the following equations:

- "Jakes" spectrum

$$P_\eta[d] = \frac{1}{\pi d_1 \Delta\nu \sqrt{1-(d/d_1)^2}}, |d| \leq d_1 \qquad (19)$$

- "Flat" spectrum

$$P_\eta[d] = \frac{1}{2 d_1 \Delta\nu}, |d| \leq d_1 \qquad (20)$$

- "Rice" spectrum

$$P_\eta[d] = \frac{A_\mathrm{a}}{\pi d_1 \Delta\nu \sqrt{1-(d/d_\mathrm{m})^2}}, d_1 \leq d \leq d_2, \qquad (21)$$

where

$$A_\mathrm{a} = \frac{\pi}{2[\arcsin(d_2/d_\mathrm{m}) - \arcsin(d_1/d_\mathrm{m})]}.$$

These equations are used in MATLAB to simulate the Doppler frequency in a TDL model, where $\eta_{d_i} = d_i \Delta\eta$, being $d_i \in [-N_\mathrm{s}/2; N_\mathrm{s}/2-1]$, $i = 1, 2$ and $d_\mathrm{m} = N_\mathrm{s}/2 - 1$. Also, these free variables (η_{d_1} and η_{d_2}) are calculated applying a threshold to $\hat{P}_{\eta_i}[d]$ between 20 dB and 30 dB with respect to its peak value.

The model complexity of the Doppler spectrum is increased with the number of free variables considered in the model. The number of free variables are two for the "Jakes" and "Flat" models, while it is four for the "Rice" model. The spectral shape shown in Table II for each proposed channel model, is determined by minimizing the mean squared error between $\hat{P}_\eta[d]$ and each $P_\eta[d]$ from the pool of models. Please note that our procedure disregards the difference in model complexity.

APPENDIX B
CONFIDENCE INTERVAL

Given a population $X = \{x_1, x_2, ..., x_{N_\mathrm{x}}\}$ with N_x elements [42], the confidence interval I_x for mean of X with a confidence of $100 \cdot (1 - 2 \cdot \psi)$ % is given by

$$I_\mathrm{x} = [\hat{m}_\mathrm{x} - \epsilon_\mathrm{x}; \hat{m}_\mathrm{x} + \epsilon_\mathrm{x}] = \hat{m}_\mathrm{x} \mp \epsilon_\mathrm{x}, \qquad (22)$$

where

$$\epsilon_\mathrm{x} = t_{N_\mathrm{x}-1,\psi} \cdot \frac{\hat{S}_\mathrm{x}}{\sqrt{N_\mathrm{x}}} \qquad (23)$$

is the maximum error in the estimate for the confidence level used. In addition, $\hat{m}_\mathrm{x}$ and $\hat{S}_\mathrm{x}$ represent an estimate of the mean and the standard deviation of X. Furthermore, $t_{a,b}$ represents the t-student distribution with degree of freedom a and probabilistic sample b.

Table VI and VII show the confidence interval for the proposed TDL models MD1 and MD5 with 95 % of confidence ($\psi = 0.025$), respectively. Where (22) has been applied to amplitude $a_{i,q}$, delay $\tau_{i,q}$ and k-factor $k_{i,q}$ for each i^{th} resolvable tap, being $\{N_a, N_\tau, N_k\} \leq Q$. In addition, ε_τ for each tap in both models are smaller than the tap resolution $R_\tau = 100$ ns used in the TDL model, so ε_τ would not cause significant errors between the estimated and simulated delay component in the model.

TABLE VI
CONFIDENCE INTERVAL FOR THE MD1 PROPOSED TDL MODEL WITH 95 % CONFIDENCE.

Taps	N_a	I_a **(dB)**	N_τ	I_τ **(ns)**	N_k	I_k **(dB)**
1	43	0.0 ∓ 0.2	43	0 ∓ 4	43	12.5 ∓ 2.0
2	43	-17.3 ∓ 1.1	43	58 ∓ 2	43	-6.0 ∓ 3.0
3	37	-21.5 ∓ 0.8	37	178 ∓ 4	43	0.5 ∓ 1.5
4	25	-24.8 ∓ 2.0	25	260 ∓ 8	43	-0.0 ∓ 2.5
5	13	-30.2 ∓ 1.1	13	380 ∓ 12	43	-4.5 ∓ 3.5
6	10	-28.4 ∓ 2.1	10	460 ∓ 14	43	-4.0 ∓ 4.0
7	2	-29.9 ∓ 2.2	2	538 ∓ 38	43	-3.0 ∓ 2.5

TABLE VII
CONFIDENCE INTERVAL FOR THE MD5 PROPOSED TDL MODEL WITH 95 % CONFIDENCE.

Taps	N_a	I_a **(dB)**	N_τ	I_τ **(ns)**	N_k	I_k **(dB)**
1	48	0.0 ∓ 0.3	48	0 ∓ 2	48	4.0 ∓ 2.0
2	48	-8.1 ∓ 0.9	48	106 ∓ 2	48	-8.5 ∓ 3.0
3	45	-11.6 ∓ 0.8	45	200 ∓ 2	48	-7.5 ∓ 2.5
4	38	-14.2 ∓ 0.4	38	308 ∓ 4	48	-7.0 ∓ 3.0
5	34	-15.7 ∓ 0.7	34	408 ∓ 4	48	-7.0 ∓ 3.0
6	31	-15.7 ∓ 0.7	31	514 ∓ 2	48	-3.5 ∓ 2.5
7	31	-16.4 ∓ 0.9	31	608 ∓ 6	48	-1.5 ∓ 2.0
8	24	-18.2 ∓ 0.7	24	706 ∓ 6	48	-3.0 ∓ 2.0
9	21	-19.2 ∓ 0.9	21	808 ∓ 6	48	-3.0 ∓ 3.0
10	16	-20.2 ∓ 0.5	16	908 ∓ 6	48	-2.5 ∓ 2.5
11	13	-20.7 ∓ 0.9	13	1 006 ∓ 8	48	-5.0 ∓ 3.0
12	12	-21.5 ∓ 0.7	12	1 110 ∓ 6	48	-4.5 ∓ 2.5
13	12	-22.8 ∓ 1.3	12	1 214 ∓ 6	48	-3.0 ∓ 2.5
14	12	-21.9 ∓ 1.6	12	1 310 ∓ 8	48	-4.5 ∓ 2.5
15	10	-20.3 ∓ 1.3	10	1 414 ∓ 10	48	-3.5 ∓ 3.0
16	6	-22.5 ∓ 0.9	6	1 502 ∓ 16	48	-3.0 ∓ 3.0

ACKNOWLEDGMENT

This contribution has been supported by both InSecTT (https://www.insectt.eu/) and SCOTT (www.scott-project.eu). InSecTT has received funding from the ECSEL Joint Undertaking (JU) under grant agreement No 876038. SCOTT has received funding from the Electronic Component Systems for European Leadership JU under grant agreement No 737422. This Joint Undertaking receives support from the European Union's Horizon 2020 research and innovation programme and Austria, Spain, Finland, Ireland, Sweden, Germany, Poland, Portugal, Netherlands, Belgium, Norway.

Also, this work has been supported by the Dept. of Economic Development and Infrastructure of the Basque Government through the project AUTOLIB (ref KK-2019/00035)

and its follow-up AUTOEV@L (ref KK-2021/00123). The document reflects only the author's view and the Commission is not responsible for any use that may be made of the information it contains.

REFERENCES

[1] S. Sand, P. Unterhuber, M. Soliman, A. Lehner, F. Berens, and J. M. García-Loygorri, "Railway Use Cases for NGV," in *IEEE NGV Meeting*, 2018, p. 12. [Online]. Available: https://mentor.ieee.org/802.11/documents?is%5C_group=00bd

[2] P. Unterhuber, S. Sand, M. Soliman, B. Siebler, A. Lehner, T. Strang, and D. Gera, "Wide band propagation in train-to-train scenarios - Measurement campaign and first results," in *2017 11th European Conference on Antennas and Propagation, EUCAP 2017*, 2017, p. 5.

[3] B. Sadeghi, "802.11bd Specification Framework Document," in *IEEE Meeting NGV*, 2019, p. 9. [Online]. Available: https://mentor.ieee.org/802.11/documents

[4] M. Berbineau, R. Behaegel, J. M. Garcia-Loygorri, R. Torrego, R. D'errico, A. Sabra, Y. Yan, and J. Soler, "Channel models for performance evaluation of wireless systems in Railway environments," *IEEE Access*, vol. 4, pp. 1–17, 2021.

[5] P. Kyösti, J. Meinilä, L. Hentilä, X. Zhao, T. Jämsä, C. Schneider, M. Narandzić, M. Milojević, A. Hong, J. Ylitalo, V.-M. Holappa, M. Alatossava, R. Bultitude, Y. de Jong, and T. Rautiainen, "LST-4-027756 Winner II Channel Model," pp. 1–206, 2007. [Online]. Available: http://projects.celtic-initiative.org/WINNER+/WINNER2-Deliverables/D4.6.1.pdf

[6] C. Wang, A. Ghazal, B. Ai, Y. Liu, and P. Fan, "Channel Measurements and Models for High-Speed Train Communication Systems: A Survey," *IEEE Communications Surveys and Tutorials*, vol. 18, no. 2, pp. 974–987, 2016.

[7] B. Ai, X. Cheng, T. Kürner, Z. Zhong, K. Guan, R. He, L. Xiong, D. Matolak, D. Michelson, and C. Briso, "Challenges Toward Wireless Communications for High-Speed Railway," *IEEE Transactions on Intelligent Transportation Systems*, vol. 15, no. 5, pp. 2143–2158, 2014.

[8] C. García, A. Lehner, T. Strang, and K. Frank, "Channel model for train to train communication using the 400 MHz band," in *IEEE Vehicular Technology Conference*, 2008, p. 5.

[9] T. Strang, A. Festag, A. Vinel, R. Mehmood, C. Garcia, and M. Röckl, "Measurement and Analysis of the Direct Train to train Propagation Channel in the 70 cm UHF-Band," in *International Workshop on Communication Technologies for Vehicles*, vol. 6596, 2011, pp. 45–57.

[10] P. Unterhuber, S. Pfletschinger, S. Sand, M. Soliman, T. Jost, A. Arriola, I. Val, C. Cruces, J. Moreno, J. P. García-Nieto, C. Rodríguez, M. Berbineau, E. Echeverría, and I. Baz, "A Survey of Channel Measurements and Models for Current and Future Railway Communication Systems," *Mobile Information Systems*, vol. 2016, 2016.

[11] P. Liu, B. Ai, Y. Li, and R. Sun, "Urban Viaduct Channel Characterization of train to train communication at 900 MHz," in *Multimedia and Ubiquitous Engineering, Lecture Notes in Electrical Engineering*, 2014, vol. 308, pp. 353–360.

[12] A. Alonso-Gómez, E. Mozo, L. Bernado, S. Zelenbaba, T. Zemen, F. Parrilla, and A. Alberdi, "Performance analysis of ITS-G5 for smart train composition coupling," in *Proceedings of 2018 16th International Conference on Intelligent Transport System Telecommunications*, 2018, p. 7.

[13] A. Lehner, T. Strang, and P. Unterhuber, "Direct train-to-train communications at low UHF frequencies," *IET Microwaves, Antennas and Propagation*, vol. 12, no. 4, pp. 486–491, 2018.

[14] S. Zelenbaba, L. Mayer, E. Mozo, F. Wirth, R. Hladik, A. Alonso-Gómez, L. Bernad, M. Schiefer, and T. Zemen, "Characterization of Time-Variant Wireless Channels in Railway Communication Scenarios," in *IEEE 2nd 5G World Forum (5GWF)*, 2019, p. 6.

[15] P. Unterhuber, M. Walter, U. Fiebig, and K. Thomas, "Stochastic Channel Parameters for Train-to-Train Communications," *IEEE Open Journal of Antennas and Propagation*, vol. 2, pp. 778–792, 2021.

[16] T. Rappaport, *Wireless Communications: Principles and Practices*. Prentice Hall, 1999.

[17] ETSI, "TR 103 257-1 V1.1.1 Intelligent Transport Systems (ITS). Access Layer. Part 1: Channel Models for the 5,9 GHz frequency band." Tech. Rep., 2019.

[18] A. Molisch, F. Tufvesson, J. Karedal, and C. Mecklenbrauker, "Propagation aspects of vehicle-to-vehicle communications - an overview," in *2009 IEEE Radio and Wireless Symposium*, 2009, p. 4.

[19] L. Bernado, T. Zemen, F. Tufvesson, A. Molisch, and C. Mecklenbrauker, "Delay and Doppler spreads of nonstationary vehicular channels for safety-relevant scenarios," *IEEE Transactions on Vehicular Technology*, vol. 63, no. 1, pp. 82–93, 2014.

[20] G. Acosta and M. Ingram, "Model development for the wideband expressway vehicle-to-vehicle 2.4 GHz channel," in *IEEE Wireless Communications and Networking Conference*, vol. 3, 2006, p. 6.

[21] M. Pätzold, *Mobile Radio Channels: Second Edition*, 2011.

[22] P. Bello, "Characterization of Randomly Time-Variant Linear Channels," *IEEE Transactions on Communications Systems*, pp. 360–393, 1963.

[23] A. Molisch, *WIRELESS COMMUNICATIONS*, John Wiley, Ed., 2011.

[24] M. Pätzold, A. Szczepanski, and N. Youssef, "Methods for modeling of specified and measured multipath power-delay profiles," *IEEE Transactions on Vehicular Technology*, vol. 51, no. 5, pp. 978–988, 2002.

[25] J. Sykora, "Tapped delay line model of linear randomly time-variant WSSUS channel," *Electronics Letters*, vol. 36, no. 19, 2000.

[26] P. Unterhuber, M. Walter, and T. Kürner, "Influence of Railway Infrastructure on Train-To-Train Communications," in *2021 15th European Conference on Antennas and Propagation (EuCAP)*, Dusseldorf, Germany, 2021, p. 5.

[27] A. Paier, J. Karedal, N. Czink, H. Hofstetter, C. Dumard, T. Zemen, F. Tufvesson, A. Molisch, and C. Mecklenbräuker, "Car-to-car radio channel measurements at 5 GHz: Pathloss, power-delay profile, and delay-Doppler spectrum," in *Proceedings of 4th IEEE Internatilonal Symposium on Wireless Communication Systems*, 2007, p. 5.

[28] G. Acosta-marum, "Measurement , Modeling , and OFDM Synchronization for the Wideband Mobile-to-Mobile Channel Measurement , Modeling , and OFDM Synchronization for the Wideband Mobile-to-Mobile Channel," *Test*, 2007.

[29] W. Mohr, "Wideband Mobile Radio Channels Based on Propagation Measurements," in *Proceedings of 6th International Symposium on Personal, Indoor and Mobile Radio Communications*, vol. 6, no. 2, 1995, pp. 397–401.

[30] X. Zhao, J. Kivinen, and P. Vainikainen, "Tapped delay line channel models at 5.3 GHz in indoor environments," in *IEEE Vehicular Technology Conference Fall*, 2000, p. 5.

[31] L. Greenstein, D. Michelson, and V. Erceg, "Moment-Method Estimation of the Ricean," *IEEE Communications Letters*, vol. 3, no. 6, pp. 175–176, 1999.

[32] K. Talukdar and W. Lawing, "Estimation of the parameters of the Rice distribution," *Journal of the Acoustical Society of America*, vol. 89, no. 3, pp. 1193–1197, 1990.

[33] M. Walter, D. Shutin, and U. Fiebig, "Delay-dependent doppler probability density functions for vehicle-to-vehicle scatter channels," *IEEE Transactions on Antennas and Propagation*, vol. 62, no. 4, pp. 2238–2249, 2014.

[34] X. Zhao, K. Jarmo, V. Pertti, and S. Kari, "Characterization of Doppler Spectra for Mobile Communications at 5.3 GHz," *IEEE Transactions on Vehicular Technology*, vol. 52, no. 1, pp. 14–23, 2003.

[35] A. Dakic, M. Hofer, B. Rainer, S. Zelenbaba, L. Bernado, and T. Zemen, "Real-Time Vehicular Wireless System-Level Simulation," *IEEE Access*, vol. 9, pp. 1–17, 2021.

[36] T. Zemen, L. Bernadó, and N. Czink, "Iterative Time-Variant Channel Estimation for 802 . 11p Using Generalized Discrete Prolate Spheroidal Sequences," *IEEE Transaction on Vehicular Technology*, vol. 61, no. 3, pp. 1–12, 2012.

[37] B. Sun, "NGV SG Use Cases (Next Generation V2X Study Group)," in *IEEE NGV Meeting*, 2018, p. 17. [Online]. Available: https://mentor.ieee.org/802.11/documents?isJuly 2020).

[38] B. Bloessl, M. Segata, C. Sommer, and F. Dressler, "Performance Assessment of IEEE 802.11p with an Open Source SDR based Prototype," *IEEE Transaction on Mobile Computing*, vol. 17, no. 5, p. 14, 2018.

[39] S. Sand, P. Unterhuber, M. Soliman, M. Schmidhammer, and F. Ponte-Muller, "Performance Analysis of Outer RS Coding Scheme," in *IEEE NGV Meeting*, 2019. [Online]. Available: https://mentor.ieee.org/802.11/dcn/19/11-19-0364-00-00bd-performance-analysis-of-outer-rs-coding-scheme.pptx

[40] S. Ioannis, "Considerations on NGV PHY design," in *IEEE Meeting NGV*, 2019, p. 25. [Online]. Available: https://mentor.ieee.org/802.11/documents?is5C_group=00bd

[41] T. Domínguez, J. Rodríguez, J. García, and L. Castedo, "Experimental Characterization of LTE Wireless Links in High-Speed Trains," *Wireless Communications and Mobile Computing*, vol. 2017, p. 21, 2017.

[42] K. Chu, S. Dean, and B. Illowsky, *Elementary statistics*, 2006, vol. 207. [Online]. Available: http://cnx.org/content/col10966/1.4/

Erislandy Mozo Bigñotte received his M.Sc degree in Telecommunication from Simón Bolívar University (USB) in 2017 in Venezuela, and the B.Sc degree in Telecommunication and Electronic Engineering from University of Oriente in Cuba. Since 2018, he was member of the Signal Theory and Communication Research Group at Mondragon Unibertsitatea, where he obtained the Ph.D. degree in Electrical Engineering in 2022. He was a visiting researcher at the Institute of Communications and Navigation in the German Aerospace Center (DLR) in 2020. His research interests are related to the design and evaluation of link-level wireless communication protocols and channel modelling with a focus on vehicular communications.

Paul Unterhuber (M'17) received the M.Sc. degree in electrical engineering and the M.Sc. degree in engineering and business from the Graz University of Technology, Graz, Austria in 2013 and 2014, respectively. Since 2015, he has been with DLR. He has participated in several national and international research projects, e.g. SBDist, V2X-DuRail, Roll2Rail and X2-Rail. His research interests are on channel sounding, propagation and modelling with a focus on train-to-train communications. He is currently a voting member of IEEE 802.11 and contributed to the IEEE 802.11bd and ETSI RT JTFIR standardization bodies.

Arrate Alonso Gómez was born in Bilbao (Basque Country), Spain, in 1985. She received the M.Sc. degree in Telecommunications engineering from ESIDE, University of Deusto, Bilbao, in 2008. In 2009, she specialized in Signal Theory at the Universidad Politécnica de Valencia (UPV), Valencia (Spain), where she received the M.Sc. degree in Communication Technology, Systems and Networks. In 2013, she received the Dr.- Tech. degree (with honours), with a Ph.D. thesis on Medium Access-Control layer protocol design (optimization) for vehicular communications, specifically for delay-sensitive and safety-related applications. Then, she joined the MOBI group (MOBI Mobility, Logistics and Automotive Technology Research Center) at the Vrije Universiteit Brussel, Brussels, Belgium, as a Postdoctoral Researcher in connected and electric mobility strategies. She participated in the European Coordination Action Smart EV-VC and coordinated the EU Project GO4SEM. Since September 2015, she has been a Researcher and Lecturer at EPS-MU, Arrasate-Mondragon, Spain, and a member of Signal Theory and Communications research team from the Computing and Electronics Department. At EPS-MU she has been main researcher of the SCOTT project (ECSEL-2016 the AUTOLIB (Elkartek 2019) project, where the performance of ITS-G5 is has been evaluated for Autonomous Train Operation. She is currently main researcher of the InSecTT project (ECSEL-2019) the AUTOEV@L (Elkartek 2021) projects, where the performance of ITS-G5, C-V2X and 802.11bd multi-Radio Access Technologies are evaluated for Intelligent Automation Services for Smart Transportation scenarios.

Stephan Sand (SM'10) received the M.Sc. in Electrical Engineering from the University of Massachusetts Dartmouth, MA, USA in 2001, the Dipl.-Ing. in Communications Technology from the University of Ulm, Germany in 2002, and the Dr. Sc. from the Swiss Federal Institute of Technology (ETH) Zurich, Switzerland in 2010. Since 2002, he has been working in several national and international research projects on wireless communications and multi-sensor navigation at the Institute of Communications and Navigation of DLR. Currently, he is leading the Vehicular Applications Group researching novel systems that combine robust navigation and wireless communications technologies. These systems will protect vulnerable road users and increase traffic efficiency and safety in railways. Since 2022, he has been teaching the lecture Navigation and Localization Techniques at the Karlsruhe Institute of Technology, Germany. Dr. Sand has authored and co-authored more than 100 publications in conferences and journals and obtained several patents on his inventions. He is an active member in worldwide and European standardization bodies, e.g., contributing to the IEEE 802.11bd Enhancements for Next Generation V2X amendment.

Mikel Mendicute Errasti (M'10, SM'19) received the B.Sc., M.Sc. and Ph.D. degrees in Electrical Engineering from Mondragon Unibertsitatea in 2000, 2003 and 2008, respectively. He was with the Communications Area of Ikerlan Research Center, from 1998 to 2003, where he worked on the development of communications devices and embedded systems. From 2003, he has been with the Signal Theory and Communications Research Group, Department of Electronics and Computer Science, of Mondragon Unibertsitatea, where he is now the Head of the Signal Theory and Communications Research Group. He was a visiting researcher at the Institute for Digital Communications of the University of Edinburgh and at the Telecommunications Circuits Laboratory of the Swiss Federal Institute of Technology (EPFL) in 2004 and 2011, respectively. His current research interests include the design and implementation of digital signal processing algorithms for communications, monitoring and embedded systems with a focus on critical wireless communication interfaces for industrial and vehicular communications.